THE ASTROPHYSICAL JOURNAL, 416:L37–L40, 1993 October 10

DISCOVERY OF INTERSTELLAR WATER LINES AT 437, 439, AND 471 GHz: STRONG CASE FOR WATER MASER FORMATION BEHIND C-TYPE SHOCKS

GARY J. MELNICK AND KARL M. MENTEN
Harvard-Smithsonian Center for Astrophysics, 60 Garden Street, MS 66, Cambridge, MA 02138
AND
THOMAS G. PHILLIPS AND TODD HUNTER
California Institute of Technology, Division of Physics, Mathematics, and Astronomy, MS 320-47, Pasadena, CA 91125
Received 1993 June 3; accepted 1993 July 23

ABSTRACT

We report the first astronomical detections of the $7_{53} \rightarrow 6_{60}$, $6_{43} \rightarrow 5_{50}$, and $6_{42} \rightarrow 5_{51}$ transitions of water vapor (H_2O) at frequencies near 437, 439, and 471 GHz, respectively. Using the Caltech Submillimeter Observatory we detected the 439 and 471 GHz lines toward a number of star-forming regions and the 437, 439, and 471 GHz lines toward several evolved stars. Maser action is likely to be present in all of these lines. The previously detected 325 GHz $5_{15} \rightarrow 4_{22}$ H_2O maser line was also observed toward these sources. Assuming that these transitions are collisionally pumped, as is almost certainly the case for the water masers in star-forming regions, the luminosity ratios of these newly discovered masers, along with the 325 GHz maser line, clearly indicate that the gas temperature within the masing region is $\gtrsim 900$ K. This finding is inconsistent with models that predict that H_2O masers form behind fast (≥ 50 km s^{-1}) dissociative shocks. Instead, these new data suggest that slow (≤ 50 km s^{-1}) nondissociative shocks are a more probable source for the observed maser emission.

Subject headings: circumstellar matter — masers — molecular processes — shock waves — stars: late-type

1. INTRODUCTION

The physical conditions that give rise to astronomical water masers have been a source of speculation since their first detection in 1968 (Cheung et al. 1969). Heretofore this speculation has been based largely upon model calculations that demonstrate that collisional pumping within dense ($n_{H_2} \sim 10^8$–10^{10} cm^{-3}) gas can produce luminous water maser emission (e.g., de Jong 1973). High masing gas densities have also been inferred from the lack of significant dynamical friction between moving maser clumps and the surrounding medium as evidenced by the small, long-term changes observed in both the lateral and line-of-sight accelerations of select 22 GHz $6_{16} \rightarrow 5_{23}$ maser spots (e.g., Genzel et al. 1981). Unfortunately, aside from permitting broad limits to be set on the density, the data provided by the 22 GHz line alone are insufficient for purposes of isolating other important properties of the masing gas, such as its temperature. However, with the discovery of several millimeter and submillimeter water maser lines during the last few years (Menten, Melnick, & Phillips 1990a; Cernicharo et al. 1990; Menten et al. 1990b), the possibility of directly determining gas properties from the strengths of the masing transitions has greatly improved.

Following the discovery of the $10_{29} \rightarrow 9_{36}$ 321 GHz water maser (Menten et al. 1990a) from several circumstellar and star-forming regions, Neufeld & Melnick (1990, hereafter NM90) investigated ways in which the 22 and 321 GHz line emissivities might constrain conditions in the masing gas. Based on the 22/321 GHz emissivity ratios measured toward five star-forming regions, NM90 concluded that the *minimum* masing gas temperature must be 200–700 K. This result was tantalizing since it was the first observational indication that models placing water masers in the regions behind fast dissociative (J-type) shocks may not be entirely adequate, because such models require that the kinetic temperature be in the range of 300 to 400 K (e.g., Elitzur, Hollenbach, & McKee 1989, hereafter EHM). As suggested by NM90, nondissociative C-shock models allowing higher gas temperatures might be necessary. However, it was recognized that additional water maser transitions would have to be observed in order to further narrow the range of conditions. Based on the predictions that the $6_{43} \rightarrow 5_{50}$ 439 GHz and $6_{42} \rightarrow 5_{51}$ 471 GHz transitions will mase below 1000 K and the possibility that under favorable weather conditions these lines could be observed from the ground (Neufeld & Melnick 1991, hereafter NM91), the 439 and 471 GHz masers were sought.

In this *Letter* we report the first detections of the 439 GHz $6_{43} \rightarrow 5_{50}$ and 471 GHz $6_{42} \rightarrow 5_{51}$ masing transitions toward both star-forming regions and evolved stars and the 437 GHz $7_{53} \rightarrow 6_{60}$ masing transition toward late-type stars. In addition, we have measured the previously detected 325 GHz $5_{15} \rightarrow 4_{22}$ maser line (Menten et al. 1990b) toward most of these sources.

Whereas water maser emission from circumstellar regions can arise from collisional excitation, radiative excitation, or line-overlap, the situation in star-forming regions is considerably more straightforward; collisions are believed to be the dominant means of excitation. For this reason, we restrict our efforts in this *Letter* to constraining the maser gas conditions in star-forming regions. In particular, we show that if it is assumed that the 325, 439, and 471 GHz masers originate within the same gas, are approximately equally beamed, and are saturated, the ratios of maser luminosities require gas temperatures in excess of 900 K. In addition, these maser line strength ratios tightly limit the combined quantity of density, water abundance, and velocity gradient within the masing gas. As discussed below, these findings strongly suggest that the

TABLE 1

OBSERVED H_2O TRANSITIONS

Transition	Frequency[a] (MHz)	E_l[b] (cm^{-1})	Sideband[c]
$5_{15} \rightarrow 4_{22}$	325152.919 (150)	315.8	USB
$7_{53} \rightarrow 6_{60}$	437346.667 (150)	1045.1	LSB
$6_{43} \rightarrow 5_{50}$	439150.812 (150)	742.1	USB
$6_{42} \rightarrow 5_{51}$	470888.947	742.1	USB

[a] Rest frequencies are taken from De Lucia et al. 1972. Numbers in parentheses give uncertainties in the last digits.

[b] Energy above the ground state of the lower energy level.

[c] Receiver sideband centered on the rest frequency of the respective H_2O transition. If the line was measured in the LSB (USB), the image sideband was at a 2.8 GHz higher (lower) frequency.

water masers we have observed are formed in the wake of slow, nondissociative C-shocks rather than behind faster, dissociative J-shocks.

2. OBSERVATIONS AND RESULTS

The four water transitions listed in Table 1 were observed between 1992 March 28 and April 1 using the 10.4 m telescope of the Caltech Submillimeter Observatory on Mauna Kea, Hawaii, under very good weather conditions. Two different liquid-helium–cooled SIS mixer receivers were used, one to observe the 325 GHz transition, the other to observe the three higher frequency transitions. The receivers were operated in double-sideband mode with one sideband, as specified in Table 1, centered on one of the H_2O lines. The data were taken in position switching mode and initially calibrated using the chopper wheel method. Subsequently, the two-step process described by Menten et al. (1990a) was employed to correct for the miscalibration caused by the fact that in general the atmospheric attenuation in the lower sideband was different from the upper sideband value. The resulting corrected antenna temperatures were converted into Jy units by assuming aperture efficiencies of 0.45 and 0.26 at 325 and 437–471 GHz, respectively. Overall, we estimate our absolute calibration to be accurate to within $\approx 40\%$. The pointing was checked by observations of planets and found to be accurate to within $\approx 5''$. The beamsize was 16″ (FWHM). The spectral lines were detected with a 1024 channel acousto-optic spectrometer with a bandwidth of ≈ 500 MHz, a channel spacing of ≈ 0.5 MHz, and effective velocity resolutions 1.5 and 1.1 km s^{-1} at 325 and 437–471 GHz, respectively.

Spectra of the 325, 439, and the 471 GHz water maser lines toward the Galactic star-forming regions G34.3 − 0.2, W49N, and Sgr B2(M) along with spectra of the 325, 437, 439, and 471 GHz maser lines toward the Mira variable U Her are shown in Figure 1. Observations of these lines toward various other evolved stars will be presented in a future paper. The positions, flux densities, and LSR velocity of the strongest features for all of the observed sources are summarized in Table 2.

3. MODEL CALCULATIONS

To obtain the saturated maser emissivities, the equilibrium level populations of all ortho and para rotational levels of the ground vibrational state of $H_2{}^{16}O$ with energies E/k up to 7700 K have been calculated using an escape probability

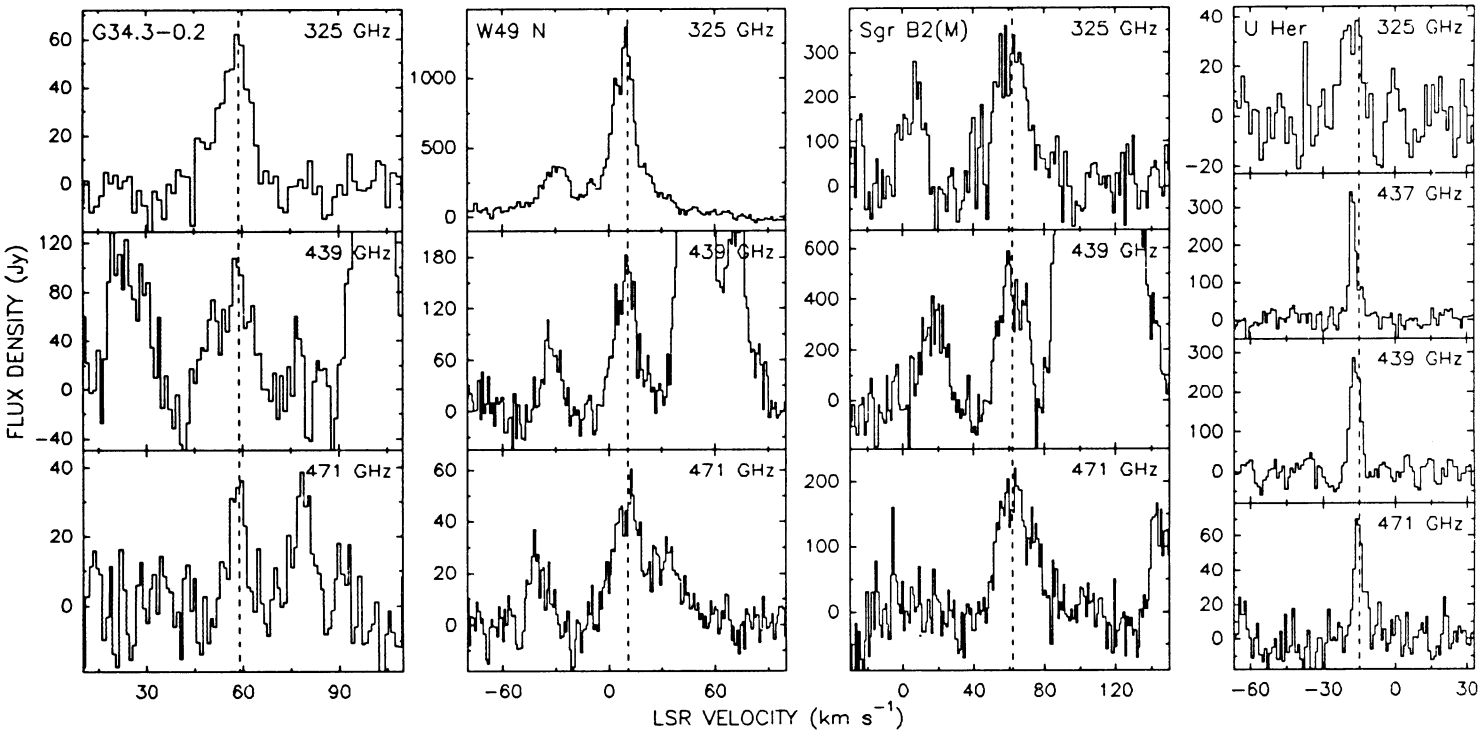

FIG. 1.—Spectra of the 325, 439, and 471 GHz H_2O transitions (*top to bottom*) observed toward the star-forming regions G34.3 − 0.2, W49 N, and Sgr B2(M) (*left three panels*). In each panel, the velocity scale is appropriate for the emission in the respective water transition, which was in all cases observed in the upper sideband (USB). The water emission appears at LSR velocities close to the systemic velocities of the sources in question. The *dashed* lines mark the velocity centroids of the water emission. In addition to the water line, in all spectra emission from other molecular lines is observed. Effective velocity resolutions are 1.52, 1.13, and 1.05 km s^{-1} for the 325, 439, and 471 H_2O lines. Spectra of the 325, 437, 439, and 471 GHz H_2O transitions toward the Mira variable U Her are also shown (*right panel*). Effective velocity resolutions are 1.52, 1.13, 1.13, and 1.05 km s^{-1} for the 325, 437, 439, and 471 GHz H_2O lines.

TABLE 2

PARAMETERS DETERMINED FROM MULTITRANSITION H_2O OBSERVATIONS

Source	α_{1950}	δ_{1950}	Transition	S_{peak} (Jy)	v_{LSR} (km s^{-1})	$\int S\,dv$ (Jy km s^{-1})	v_{LSR}-range (km s^{-1})
U Her	$16^h23^m34^s.7$	19°00′17″	$5_{15} \rightarrow 4_{22}$	37	−16	360 (50)	[−26, −12]
			$7_{53} \rightarrow 6_{60}$	340	−18	1370 (72)	[−23, −12]
			$6_{43} \rightarrow 5_{50}$	286	−17	1430 (80)	[−22, −11]
			$6_{42} \rightarrow 5_{51}$	69	−16	337 (36)	[−20, −10]
G34.3−0.2	18 50 46.4	01 11 14	$5_{15} \rightarrow 4_{22}$	64	59	690 (40)	[46, 68]
			$6_{43} \rightarrow 5_{50}$	≈110[a]	59	≈1200 (200)[a]	[46, 68][b]
			$6_{42} \rightarrow 5_{51}$	36	60	220 (50)	[51, 65]
Sgr B2(N)	17 44 10.1	−28 21 18	$5_{15} \rightarrow 4_{22}$	≈300	≈66	≈5000 (200)	≈[50, 83]
			$6_{43} \rightarrow 5_{50}$	≈380	≈65	≈4300 (730)	≈[50, 83][b]
			$6_{42} \rightarrow 5_{51}$	<180	60	<1100	
Sgr B2(M)	17 44 10.4	−28 22 02	$5_{15} \rightarrow 4_{22}$	≈300	≈60	≈6500 (450)	≈[48, 85]
			$6_{43} \rightarrow 5_{50}$	≈590	≈60	≈8400 (510)	≈[50, 75]
			$6_{42} \rightarrow 5_{51}$	≈220	≈64	≈4100 (180)	≈[48, 83]
W49 N	19 07 49.8	09 01 17	$5_{15} \rightarrow 4_{22}$	1364	10	33200 (300)	≈[−60, 70]
						23000 (200)[c]	[−10, 40]
			$6_{43} \rightarrow 5_{50}$	191	10	4170 (230)	≈[−60, 70]
						2900 (190)[c]	[−10, 40]
			$6_{42} \rightarrow 5_{51}$	54	10	1300 (50)	≈[−60, 70][d]
W51 Main	19 21 26.2	14 24 43	$5_{15} \rightarrow 4_{22}$	168	64	1750 (80)	≈[50, 70]
			$6_{43} \rightarrow 5_{50}$	70	57	570 (150)	≈[50, 70][b]
			$6_{42} \rightarrow 5_{51}$	<54	60	<250	
W51 d	19 21 22.3	14 25 15	$5_{15} \rightarrow 4_{22}$	188	63	1170 (120)	≈[53, 70]
			$6_{43} \rightarrow 5_{50}$	<90	60	<400	
			$6_{42} \rightarrow 5_{51}$	<60	60	<250	

NOTES.—S_{peak} and v_{LSR} are the peak flux density and LSR velocity of the strongest emission. Flux densitied integrated over the whole v_{LSR}-range showing emission are given by $\int S\,dv$ together with formal 1 σ errors, which are derived from the rms noise in the spectra. Systematic calibration errors are estimated to cause a 40% uncertainty in the flux density scale.

[a] Intensity very uncertain because of uncertainty in baseline level.

[b] v_{LSR}-range is difficult to determine and therefore assumed to be identical to range covered by emission in the 325 GHz $5_{15} \rightarrow 4_{22}$ line.

[c] Flux density integrated over the velocity range covered by emission in the 471 GHz $6_{42} \rightarrow 5_{51}$ line.

[d] Emission between −50 and −30 km s^{-1} (see Fig. 1) is from image sideband.

method described by NM91. Only two updates to NM91 were made in the calculations presented here: (1) for collisionally induced transitions among the lowest 45 levels of ortho- and para-water, the rate coefficients calculated by Green, Malvendes, & McLean (1993) for He-H_2O collisions were used (multiplied by 1.348 to account for the different reduced mass when H_2 is the collision partner), and (2) the expression for the photon escape probability used by Neufeld & Kaufman (1993) was adopted.

We obtain level populations for plane-parallel media in which the limit of large velocity gradient (LVG) applies. As previously noted (EHM; NM91), if the background radiation field is negligible and the gas density is $\lesssim 10^{10}$ cm^{-3}, the level populations may be written approximately as a function of two variables: the kinetic temperature T and a combination of parameters represented by the variable ξ', defined by

$$\xi' \equiv G \times x_{-4}(H_2O) n_9^2/(dv_z/dz)_{-8}\ , \qquad (1)$$

where $n = 10^9 n_9$ cm^{-3} is the density of hydrogen nuclei, $10^{-4} x_{-4}(H_2O)$ is the water abundance relative to hydrogen nuclei, and $10^{-8}(dv_z/dz)_{-8}$ cm s^{-1} cm^{-1} is the magnitude of the velocity gradient. As discussed in NM91, G is a geometrical factor which is equal to unity for the LVG slab considered here.[1]

[1] ξ appropriate to a static medium is closely related to ξ', differing only in that the velocity dispersion, Δv, and medium thickness, d, replace dv_z and dz, respectively, in eq. (1). Such a definition of ξ was introduced by EHM and is approximately related to the LVG results presented here using the substitution $\xi' = \xi_{EHM}/[3(\ln \bar{\tau})^{1/2}] \simeq \xi_{EHM}/9$, where $\bar{\tau}$ is the optical depth of a typical far-infrared water transition.

Finally, the apparent isotropic photon luminosity seen by an observer within the maser beam is just the product of the maser photon generation rate, the volume of the emitting region, and the solid angle of the maser beam. Unfortunately, the geometry and beam solid angle cannot be determined observationally. Nevertheless, making the plausible assumption that for saturated masers the beaming angles are approximately the same, varying at most by a logarithmic factor from one transition to another (cf. NM90), the observed ratio of intensities in more than one maser line can be used to determine physical conditions in the masing region without our needing to know the exact geometry. The emissivity ratios Q(325 GHz)/Q(439 GHz), Q(325 GHz)/Q(471 GHz), and Q(439 GHz)/Q(471 GHz) are plotted in Figure 2.

4. DISCUSSION

The conditions needed to produce strong water maser emission are, in many respects, extreme—gas densities must be approximately 10^9 cm^{-3} and temperatures must be greater than 100 K in order to collisionally pump the observed maser transitions. In addition, large negative optical depths must be achieved in order that there be sufficient gain to reproduce the observed maser luminosities. Such gains can only be attained along paths with small velocity gradients. To accommodate these various prerequisites, EHM have suggested that 22 GHz water masers in star-forming regions are excited by collisional pumping of dense, neutral gas which has been compressed and heated by an interstellar shock. EHM were able to account for the luminosities and brightness temperatures typically

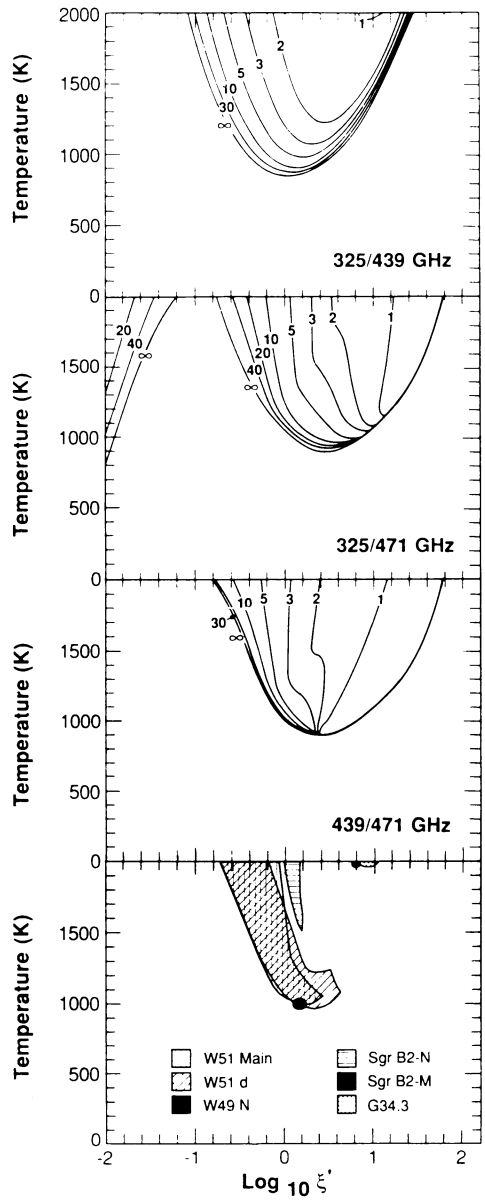

FIG. 2.—Emissivity ratio: contours of the quantity Q(325 GHz)/Q(439 GHz) (*top panel*), Q(325 GHz)/Q(471 GHz) (*middle-top panel*), and Q(439 GHz)/Q(471 GHz) (*middle-bottom panel*) are plotted as a function of ξ' and gas temperature, T. In the bottom panel, the shaded regions indicate the range of ξ' and temperature consistent with the measured emissivity ratios Q(325 GHz)/Q(439 GHz), Q(325 GHz)/Q(471 GHz), and Q(439 GHz)/Q(471 GHz) toward the galactic star-forming regions Sgr B2-N, Sgr B2-M, G34.3, W49 N, W51D, and W51 Main.

observed for interstellar 22 GHz masers by a model in which the emission is assumed to originate in velocity-coherent filaments of shocked gas at a temperature of $\sim$400 K and $\xi_{EHM} \sim$ 1–10 (or $\xi' \sim 0.1$–1). Such conditions arise naturally within a region of molecule reformation that trails the passage of a fast ($\gtrsim 50$ km s^{-1}) dissociative (J-type) shock into a gas of preshock density $\sim 10^7$ cm^{-3}. Moreover, it is a characteristic of J-shocks that their postshock regions have small velocity gradients which could foster high maser amplification gains.

The range of ξ' and T consistent with the integrated 325, 439, and 471 GHz flux densities measured for each source is plotted in Figure 2. These new data clearly show that gas temperatures less than 900 K, *regardless* of the assumed H_2 density, water abundance, or velocity gradient, cannot reproduce the observed maser luminosities. To do so, therefore, requires an alternate mechanism to dissociative shocks.

The conditions needed to account for our observations can be attained behind slower (≤ 50 km s^{-1}) nondissociative (C-type) shocks. Such an explanation is appealing for two reasons. First, the endothermic reactions which convert O and H_2 to H_2O proceed rapidly behind C-shocks, as they do behind J-shocks; most of the preshock oxygen is converted to H_2O by shocks with velocities in the range of 10 to 25 km s^{-1}. In this way, a preshock H_2O abundance of 10^{-7} (relative to H_2) can be enhanced by a factor of about 500 in the postshock region. Second, and more important, because molecules are not destroyed in C-shocks, water formed behind a C-shock survives and can reach temperatures of more than 900 K for modest velocities ($\sim$15–25 km s^{-1}). Furthermore, it is worth noting that even though the velocity gradient along the direction of shock propagation is large behind a C-shock and small behind a J-shock, along a direction perpendicular to the shock propagation both types of shocks will possess small velocity gradients. Thus, C-shocks, like J-shocks, can have gain paths sufficient to produce the luminous submillimeter water masers (cf., Kaufman & Neufeld 1993) and appear to be the likely source of the emission we observe.

Lastly, the 437 GHz line detected toward U Her was not predicted to be masing by NM91 at temperatures ≤ 1000 K. A subsequent investigation, in which temperatures up to 2000 K were considered, still does not indicate that this transition experiences a population inversion. This leads us to conclude that effects other than collisions, such as radiative pumping or line-overlap, cause the observed maser action in this line. A more detailed discussion of the conditions likely to generate water maser emission in circumstellar regions will be presented in a future paper.

The Caltech Submillimeter Observatory is funded by the National Science Foundation under contract AST-9015755.

REFERENCES

Cernicharo, J., Thum, C., Hein, H., John D., Garcia, P., & Mattioco, F. 1990, A&A, 231, L15
Cheung, A. C., Rank, D. M., Townes, C. H., Thornton, D. D., & Welch, W. J. 1969, Nature, 221, 626
de Jong, T. 1973, A&A, 26, 297
DeLucia, F. C., Helminger, P., Cook, R. L., & Goody, W. 1972, Phys. Rev. A, 5, 487, 5334
Elitzur, M., Hollenbach, D. J., & McKee, C. F. 1989, ApJ, 346, 983 (EHM)
Genzel, R., Reid, M. J., Moran, J. M., & Downes, D. 1981, ApJ, 244, 884
Green, S., Maluendes, S., & McLean, A. D. 1993, ApJ, 85, 181
Kaufman, M. J., & Neufeld, D. A. 1993, in preparation
Menten, K. M., Melnick, G. J., & Phillips, T. G. 1990a, ApJ, 350, L41
Menten, K. M., Melnick, G. J., Phillips, T. G., & Neufeld, D. A. 1990b, ApJ, 363, L27
Neufeld, D. A., & Kaufman, M. J. 1993, ApJ, in press
———. 1990, ApJ, 352, L9 (NM90)
———. 1991, ApJ, 368, 215 (NM91)